Available online at www.sciencedirect.com
SCIENCE DIRECT
Surface & Coatings Technology 200 (2005) 2547–2556
SURFACE & COATINGS TECHNOLOGY
www.elsevier.com/locate/surfcoat

Characterization of niobium, tantalum and chromium sputtered coatings on steel using eddy currents

Changqing Lee[a,*], Yaron Danon[a], Chris Mulligan[b]

[a]Department of Mechanical, Aerospace and Nuclear Engineering, Rensselaer Polytechnic Institute, Troy, NY 12180, United States
[b]Benet Laboratories, US Army, AMSTA-AR-CCB-TB, Watervliet Arsenal, NY 12189, United States

Received 8 June 2004; accepted in revised form 5 December 2004
Available online 11 March 2005

Abstract

A method that uses induced eddy current for characterization of niobium, tantalum and chromium sputtered coating on steel is presented in this paper. The objective of this work is to find the correlation between the sputtering conditions and resistivity of coatings and to develop a system for fast inspection of coatings as a coating quality control tool during production as well as in the field for determining coating degradation levels. A two-probe differential system having higher sensitivity and less noise than a one-probe system with 2D scanning ability was developed. A computer program that controls an *XY* table and performs fast data acquisition was written. Resistivity maps of the niobium, tantalum and chromium coated samples were constructed and are shown in the paper. For niobium coatings, the relationship between sputtering pressure and resistivity of coatings is examined, as well as the relationship between impurity level of process gas and resistivity of coatings. For tantalum coatings, the relationship between beta-Ta fraction and resistivity is analyzed. For chromium coatings, the relationship between micro-crack density and resistivity of coatings is analyzed. The topographic picture and destructive analysis of the samples show very good correlation with eddy currents measurements.

Keywords: Eddy currents; Sputtered coatings; Resistivity of coatings; Sputtering conditions

1. Introduction

The eddy current method can be applied to measure electrical resistivity and thickness of thin coatings on metallic material [1,2]. As a method for nondestructive inspection, eddy current techniques are also used for detection of corrosion in airplane structures and defects in metals [3–5]. Recently, we also reported an application for Ta coating surface inspection by using pulsed eddy current methods showing both the theoretical and instrumental perspectives [6,7].

Currently, the demand to increase range, rate of fire and muzzle velocity has resulted in increased wear and erosion problems in gun tubes. As a result, there has been a drive to introduce improved coatings to mitigate these problems. In support of this research, use of nondestructive eddy current techniques to characterize the structure and properties of coatings will help to advance the development and maturation of the next generation of advanced coatings for gun tubes.

The eddy current method is based on the induction of magnetic fields in a sample. These magnetic fields created by a coil will induce currents in the metal, which can be detected by a probe above the metal surface [8]. In the work described here, we use a two-probe differential system to induce the magnetic field and detect the eddy currents. The net effect of this process is to measure the change of the probe's impedance when it is coupled to the metallic surface under testing.

The eddy current technique has several advantages; it is a nondestructive and non-contact method, and as a result, no damage is done to the surface even when the scan is performed at very high speeds. Thus, it does not rely on

* Corresponding author.
E-mail address: cqlee2182@yahoo.com (C. Lee).

0257-8972/$ - see front matter © 2005 Elsevier B.V. All rights reserved.
doi:10.1016/j.surfcoat.2004.12.033

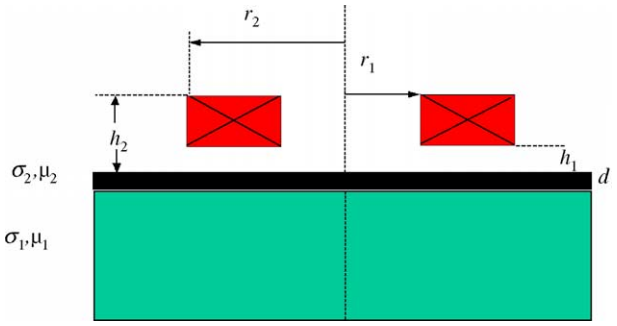

Fig. 1. An air coil over one-layer coating of thickness d.

good contact with the surface like other resistivity measurement methods such as a four-point probe. The method can accurately determine the resistivity and in some configurations also measure the coating thickness. Another advantage is that the instrumentation required for these types of testing is relatively simple and thus reliable and inexpensive.

Resistivity measurement is of special interest due to its relationship with factors affecting coating properties. For instance, the resistivity of coatings is very sensitive to changes in density and morphology. In fact, porous columnar deposited coatings with open grain boundaries can have resistivities an order of magnitude or greater than the respective bulk values for a given material [9]. In addition, resistivity is sensitive to interstitial impurities such as H, O, C and N.

Besides these relationships, in physical vapor deposited coatings, multiple phases of some materials may form with varying resistivities. This is the case for one of the primary materials under consideration for gun bore protection. The refractory metal tantalum can form two phases under physical vapor deposition: the alpha (α) phase, which is the stable bcc phase, and beta (β), which is a metastable phase. In tantalum deposited on steel, the beta (β) phase tends to form at the substrate/coating interface where adhesion is critical. This is problematic in that the beta phase is very brittle and may result in premature coating failure under applied stresses. It has been reported [7,10] that beta tantalum has a resistivity an order of magnitude greater than alpha phase tantalum (~200 μΩ cm and ~20 μΩ cm respectively). Taking this into account, it is easily perceived that an instrument that can measure the resistivity of tantalum coatings would be the most practical characterization device. Electrical resistivity measurements have been very effective for research in process control in fabrication of micro-electronic circuits [12]. However, in this application, the coating is deposited onto a conductive substrate (gun steel as opposed to silicon); therefore, measuring resistivity through traditional four-point probe measurements is not possible.

The current practice to identify and quantify concentrations of beta tantalum is through X-ray diffraction, by which direct information on the crystalline structure can be obtained [11] and/or destructive characterization. However, these methods are relatively slow, more costly, and much more difficult to execute than the method proposed by the authors, particularly outside of the lab environment.

2. Theory

The theory of eddy current testing can be derived from Maxwell's equations. The analytical solution for an air coil positioned above a one-layer coated substrate as illustrated in Fig. 1 was given by [13].

The coil inner radius is noted by r_1 and the outer radius is noted by r_2. The bottom and top distance of the coil edges from the coating are h_1 and h_2 respectively such that the coil length is given by $L=h_2-h_1$. The number of turns of the coil is denoted by n. σ_1 and σ_2 are the conductivity of the coating and the substrate respectively. μ_1 and μ_2 are the permeability of the coating and the substrate respectively. The thickness of the coatings is denoted by d.

The expression of the coil's impedance $Z(\omega)$ given by [13] is applicable for a single excitation frequency. A method that is better than the conventional methods and more suited for fast sampling of the impedance is the pulsed eddy current. The pulsed eddy current technique, which uses a step function voltage to excite the probe, is a promising approach in the field of eddy current testing. The advantage of using a step function voltage is that it contains a continuum of frequencies; as a result, the electromagnetic response to several different frequencies can be measured with just a single pulse. Since the skin depth of penetration is dependent on the frequency of excitation, information from a range of depths can be obtained simultaneously. For example, Tai et al. [2] showed that pulsed eddy current could be used to simultaneously determine the resistivity and thickness of coatings on non-magnetic substrates. However, for the work presented here, we chose to simplify the procedure and measured the thickness of the tantalum coating with the magnetic induction method. Another advantage of applying pulsed eddy currents for the purpose of repetitive scanning is that the low duty cycle of the pulses puts less average power through the small probe coils, which allows to operate at high instantaneous current during the pulse itself. For the pulsed eddy current technique, the coil will

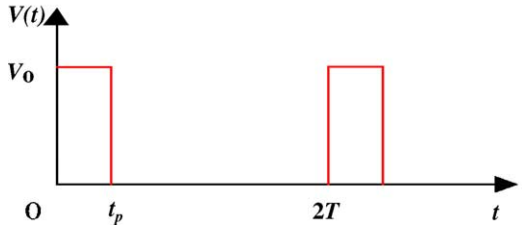

Fig. 2. Square excitation pulse with width t_p, height V_0 repeating every $2T$.

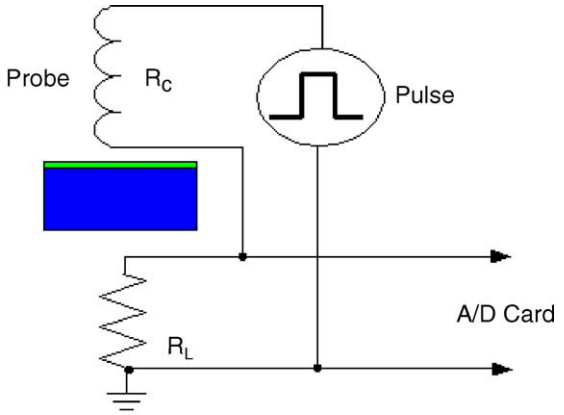

Fig. 3. Experiment setup for a one-coil system shown above a one-layer coated sample.

be excited by a square pulse of duration t_p during which we apply constant voltage V_0 to the coil. This is illustrated in Fig. 2.

In order to apply the theory developed for the impedance calculations of a coil excited by a pulse, we can first apply Fourier transformation to obtain all of the components of the pulse. After that, we can get the response of the coil from all the components. These components are added and the response of a pulse is obtained. The detailed process is given as follows.

First, a Fourier transformation of the pulse (see Fig. 2) is used.

$$V(t) = V_0\left[\frac{t_p}{2T} + \sum_{n=1}^{N}\left(a_n\cos(\omega_n t) + b_n\sin(\omega_n t)\right)\right]. \quad (1)$$

Where the Fourier coefficients a_n and b_n are given by;

$$a_n = \frac{\sin(\omega_n t_p)}{n\pi} \quad (2)$$

$$b_n = \frac{1-\cos(\omega_n t_p)}{n\pi}. \quad (3)$$

The angular frequency and frequency are given by $\omega_n = n\pi/T$ and $f_n = \omega_n/(2\pi)$ respectively. To calculate the

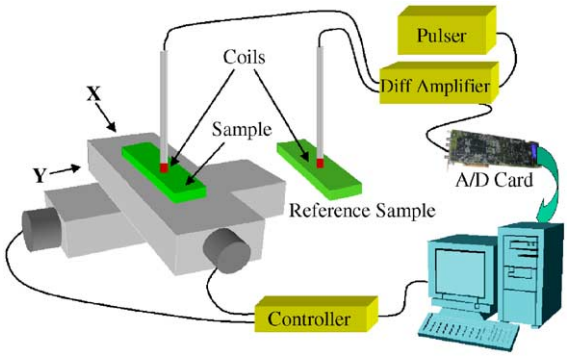

Fig. 5. An illustration of the *XY* eddy current scanner. The scanner includes an *XY* positioning system and a differential probe system.

voltage on the coil, consider the circuit in Fig. 3. Applying the relation $I=V(t)/Z(\omega)$ and using Eq. (1), the voltage that is read by the A/D board is given by,

$$V(t) = V_0 R_L\left[\frac{t_p}{2TR_T} + \sum_{n=1}^{N}\left(\frac{a_n\cos(\omega_n t-\theta(\omega_n))+b_n\sin(\omega_n t-\theta(\omega_n))}{\mathrm{Mag}(\omega_n)}\right)\right] \quad (4)$$

where $Z(\omega)$ is the impedance of the coil for each frequency, R_T is the total resistance in the circuit, including the load resistance R_L, the coil resistance R_C, and the output resistance of the pulse generator R_0. In this case the complex impedance of the coil and the real resistance of the other components were represented in polar coordinates with magnitude:

$$\mathrm{Mag}(\omega_n) = \sqrt{Im(Z(\omega_n))^2 + [Re(Z(\omega_n)) + R_t]^2} \quad (5)$$

and phase,

$$\theta(\omega_n) = \tan^{-1}\left(\frac{Im(Z(\omega_n))}{Re(Z(\omega_n)) + R_t}\right) \quad (6)$$

To achieve high sensitivity, two measurements are done. One over the sample coatings is labeled S and another over

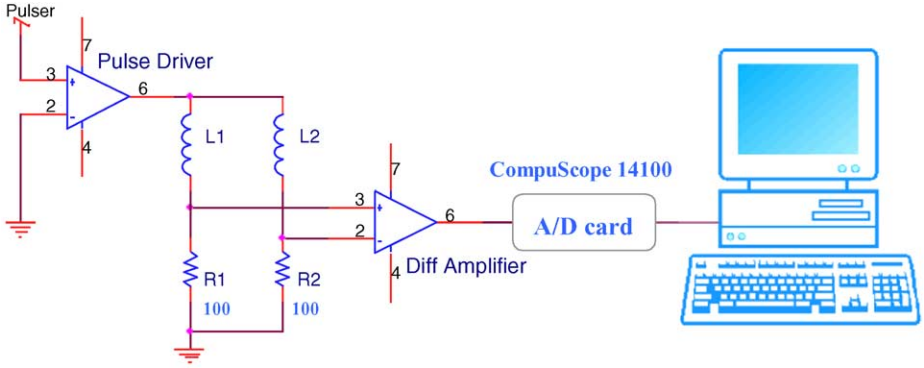

Fig. 4. Experimental setup for the differential system. Included are probe coils, pulse driver, differential amplifier and a computer DAQ.

Table 1
Test samples and deposition parameters

Series	Material	Sample	Sputtering pressure (mTorr)	Sputtering gas	Impurity levels (percent process gas [%])[a]	Coating thickness (μm)
Impurity level	Nb	Nb-A1	10	Ar	10	40.9
	Nb	Nb-A2	10	Ar	5	16.4
Sputtering pressure	Nb	Nb-1	10	Ar	1.5	49.5
	Nb	Nb-2	30	Ar	1.5	62.0
	Nb	Nb-3	40	Ar	1.5	38.1
Aqueous HC–Cr	HC–Cr	Cr-1	Plated	–	–	43.2
HC–Cr	HC–Cr	Cr-2	Plated	–	–	71.1
	HC–Cr	Cr-3	Plated	–	–	88.9
	HC–Cr	Cr-4	Plated	–	–	137.2
Beta-Ta fraction	Ta	Ta-1	30	Kr	1.5	29.5
	Ta	Ta-2	10	Kr	1.5	31.2

[a] As measured with an Inficon Residual Gas Analyzer.

the reference substrate is labeled R. The difference is given by

$$\Delta V(t) = V_S(t) - V_R(t) \tag{7}$$

The advantage of this method is that allows to differentiate a small signal $\Delta V(t)$ that is embedded in the large signal from the coil response $V_S(t)$. After obtaining data from measurements, we can convert the voltage measurements to resistivity based on a set of calibration curves [7].

3. Experiment setup

A differential system with two coils was used and is shown in Fig. 4. The differential system was driven by a Tabor-8024 waveform /function generator, and the signal is amplified by a wide band differential amplifier that was designed by the authors for this purpose. The gain of the amplifier is changeable and a factor of 5 is applied in the experiment. The output of the amplifier was connected to a 14-bit A/D card (CompuScope 14100) from Gage Applied.

The pulse driver was designed to provide the system with constant voltage with a very low internal resistance, less than 1Ω.

In order to map the resistivity of a sample, an eddy current scanner was designed and constructed as illustrated in Fig. 5. One sample was positioned on a computer controlled *XY* table and another reference sample was used as illustrated in Fig. 5. The two coils are stationary and the sample being scanned is moving under the scanning probe. This arrangement allows the system to scan the resistivity of the sample relative to the resistivity of the magnetic gun steel when it is used as the reference sample. In order to reduce inaccuracies from small differences between the two differential channels, a measurement of the system's response when the two probes are placed over the stainless steel 4340 was done first. This measurement is treated as background and was subtracted from the signal obtained from each pulse. The typical height of the probe above the surface h_1=0.5 mm. This liftoff value was kept constant during all the measurements in order to rule out the liftoff effect. In our practical experiments, the liftoff variation was kept small enough to be negligible.

Depositions of tantalum, niobium and chromium were completed on 4340 steel substrates via magnetron sputtering and electroplating. The stainless steel deposition chamber consists of a plasma cleaning station and a 2-in. diameter standard water-cooled magnetron gun. Background pressures were measured via an Inficon residual gas analyzer.

Preparation of the substrates prior to installation into the system included polishing to 2- to 3-μin. RMS surface finish. Directly prior to magnetron sputtering of each tantalum and niobium coating, the substrates were plasma cleaned in situ in Ar at a rate of ~170 Å/min for 30 min to ensure good bonding.

The parameters of each deposition are given in Table 1. Niobium was used on several depositions in lieu of tantalum due to its close relationship with tantalum and the fact that it does not form the detrimental beta phase. This allows us to differentiate and test such parameters as sputtering pressure, contamination levels, etc. without worrying about the formation of beta phase, which is unpredictable in tantalum and can change with the aforementioned sputtering parameters.

To determine the sensitivity of resistivity measurement to coating density, niobium depositions were completed at different sputtering pressures. The effects of sputtering pressure on coating density are related to atomic shadowing and increased sputtered particle collisions in the gas phase and are relatively well understood [14,15]. Depositions at

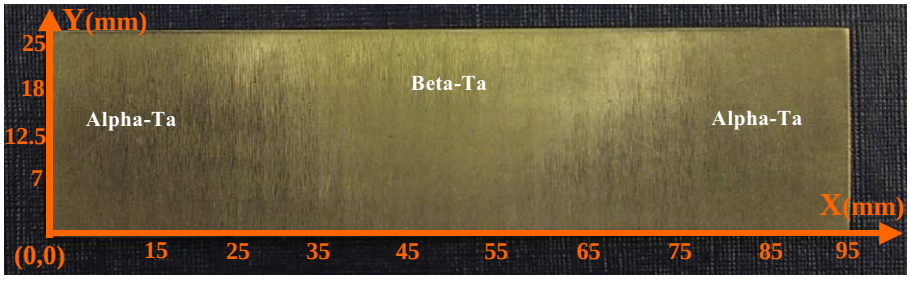

Fig. 6. Surface image illustrating the distribution of alpha (darker phase) and beta (lighter phase) tantalum across the surface of the sample.

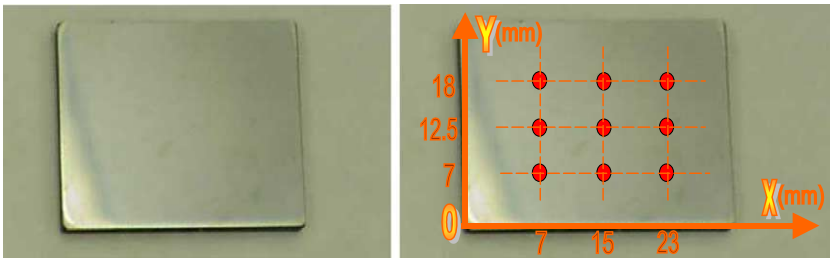

(a) (b)

Fig. 7. (a) Typical planar niobium sample deposited via magnetron sputtering, (b) niobium sample with an imaginary grid showing thickness measurement points.

10, 30, and 40 mTorr were completed. The current was held constant with each run, however there were some fluctuations in voltage and power and thus substrate temperature with increasing pressure. The temperature was monitored and based on the relatively small changes in homologous temperatures (T/T_m), it is reasonable to assume the temperature change does not play a substantial role in coating density.

To evaluate the sensitivity of eddy current resistivity measurement to impurity content, two niobium depositions were completed at 10 mTorr Ar sputtering pressure with the introduction of a controlled leak through a bleed valve on the vacuum system. The partial pressure of the background gas in relation to the sputtering gas was monitored using an Inficon Residual Gas Analyzer (RGA). The first deposition was completed with a background gas partial pressure of 10% total (or 1.0 mTorr) and the second deposition was completed with a background gas partial pressure of 5% (or 0.5 mTorr). A background gas pressure of any higher value would lead to the risk of poisoning the target and would not be a realistic representation of the level of background impurities that may be present during an actual deposition.

To determine the relationship between resistivity and beta-Ta concentration, tantalum depositions were completed in a similar manner with the following exceptions. Krypton as opposed to Argon sputtering gas was used due to the increase in beta-Ta concentration experienced in this system while sputtering in Kr. The tantalum specimen dimension was increased to 4.0 in. (102 mm) in length due to the geometry of the beta-Ta that is formed. The beta-Ta (lighter phase) tends to form directly in the center of the specimen and there is a gradual transition to alpha-Ta (darker phase) away from the center as illustrated in Fig. 6. This gives us a full range of beta-Ta concentrations to evaluate via eddy currents.

To determine the relationship between micro-crack density and resistivity in electroplated chromium coatings, four depositions were completed of varying thickness. The depositions were completed in a bath at 55 °C and a deposition rate of 12–15 μm/h. The resultant coatings contain varying concentrations of micro-cracks which are related to the coating thickness.

4. Results

For the niobium sample, an accurate thickness measurement was completed using a magnetic induction coating thickness gauge from DeFelsko. The measurement does not

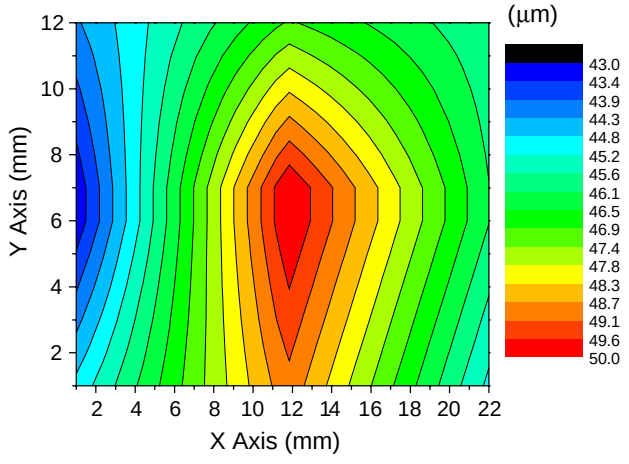

Fig. 8. Thickness map for the niobium sample interpolated from points measured using a magnetic induction thickness gauge (sample Nb-1).

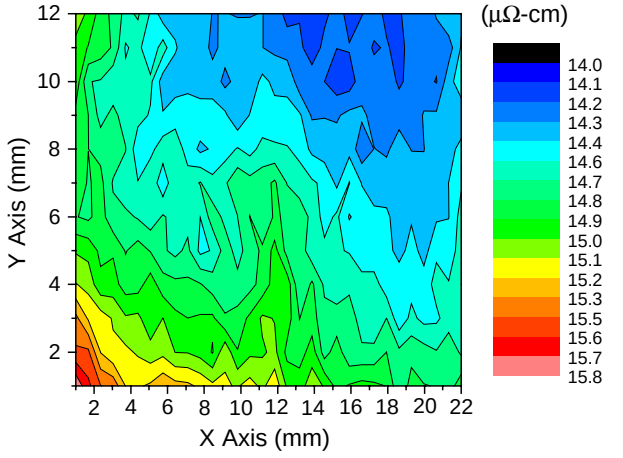

Fig. 9. Resistivity map as measured via eddy current for the niobium sample (Nb-1). The measured data were corrected for variations in the coating thickness.

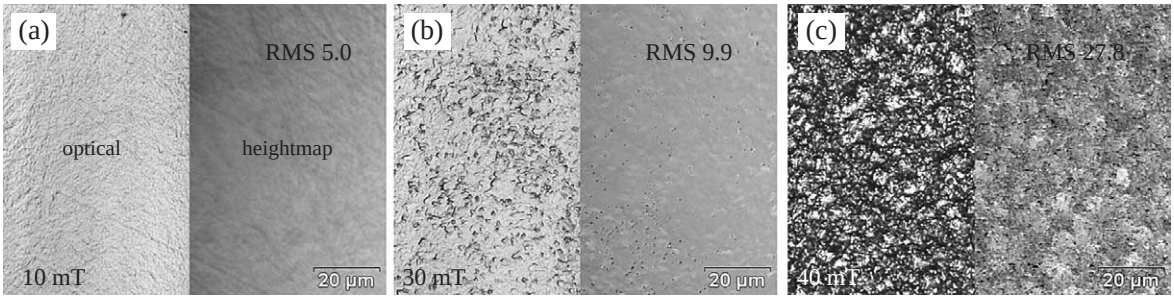

Fig. 10. Composite images combining optical (left) and topographic heightmap (right) images as measured by laser scanning confocal microscopy. The sputtering pressure and surface finish are given for each image. Note the increase in surface roughness with increasing sputtering pressure (RMS surface finish given in a.u.).

depend on the resistivity of the coating. The measurements were completed on a grid overlaid on the sample as shown in Fig. 7. A total of 9 points were measured. The thickness at an arbitrary point is obtained by linear interpolation between measured points as shown in Fig. 8. This method is sufficiently accurate when the changes in thickness are small and vary smoothly, which is typical for the samples analyzed in this work.

Fig. 8 illustrates the thickness map along the surface of the niobium coating that is generated from the linear interpolation of points measured via magnetic induction.

Fig. 9 shows a resistivity map of a niobium sample that was obtained using our eddy current scanning system and was corrected for coating thickness nonuniformity. For the correction, the thickness map and a theoretical model were utilized. Detailed discussions are available in [7].

4.1. The relationship between sputtering pressure and resistivity of coatings for niobium coatings

Three specimens (Nb-1, 2, and 3) were deposited to test the correlation of resistivity and coating density. For these

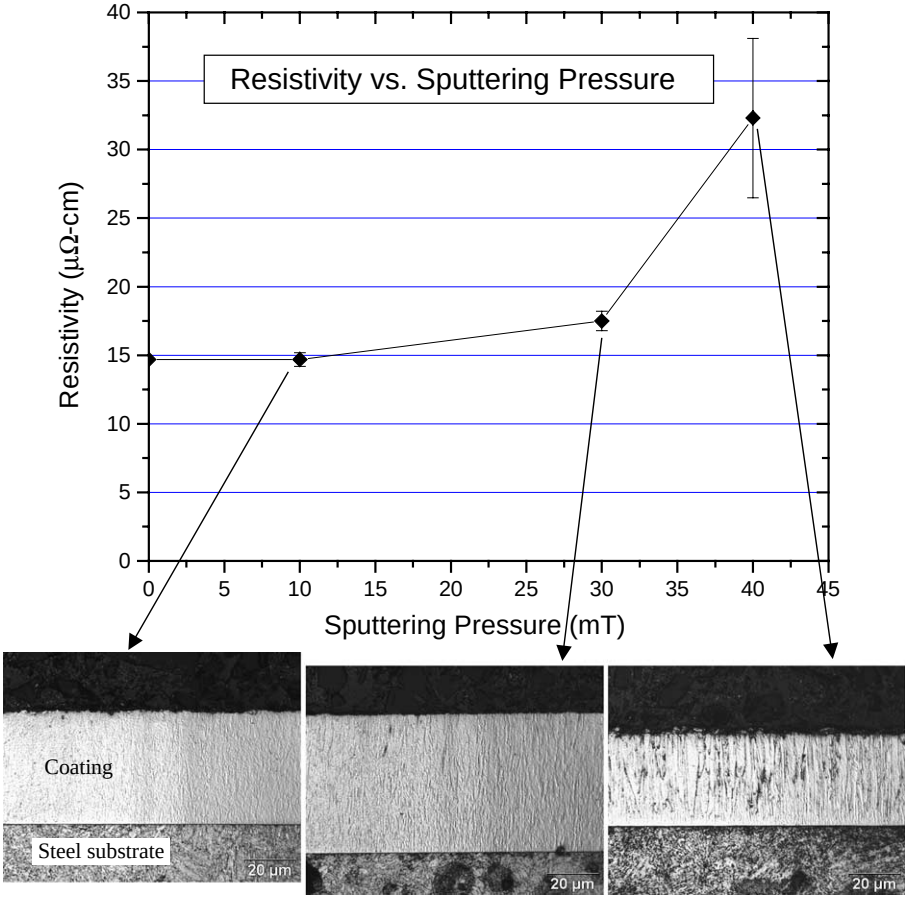

Fig. 11. Chart of the resistivity vs. sputtering pressure along with etched metallographic cross sections taken for the niobium samples sputtered at different pressures. The changes in resistivity correlate well with observed changes in coating porosity.

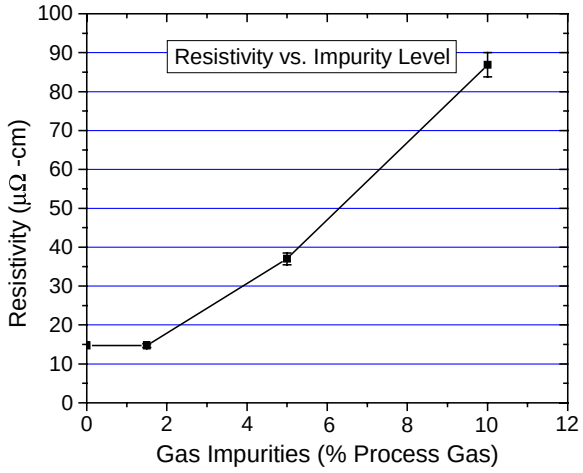

Fig. 12. Chart of resistivity vs. impurity level for niobium samples deposited at varying background gas impurity levels.

three niobium specimens, the thickness as measured by magnetic induction and the resistivity as measured by eddy current along the surface are relatively uniform. This was expected due to the fact that niobium does not form a secondary metastable phase.

Surface images and heightmaps were taken of each specimen prior to subjecting to eddy current measurement. Composite images were produced for clearer description. These are given in Fig. 10 with the optical image on the left and the associated heightmap given on the right. The surface structures correlate well with the measured changes in resistivity. As illustrated, the change in surface structure is not as drastic as one increases pressure to 30 mTorr as opposed to 40 mTorr. Inset in the images are the relative RMS surface roughnesses given in arbitrary units (a.u.) as measured by laser scanning confocal microscopy.

Furthermore, metallographic characterization of the specimens was conducted to compare resistivity values to actual structural changes. Illustrated in Fig. 11 is the plot of resistivity vs. sputtering pressure and superimposed are cross-sectional images taken from the niobium sputtered specimens following a 90-s etch in HF-H_2SO_4 etchant. The results are similar to that of the topographic analysis. The porosity noted at 40 mTorr is much more acute than that at 30 mTorr, which is in agreement with the resistivity measurements. The greater variation in the resistivity across the surface of the sample sputtered at 40 mTorr is not believed to be representative of fluctuations in the measurement system but rather actual fluctuations in the resistivity of the coating. At 40 mTorr the atomic shadowing effects are exacerbated and since a 2-in. (51 mm) diameter magnetron gun was used, the coating exhibits highest resistivity at the center point and lower resistivity at the edges as the oblique flux component plays more of a role in the shadowing effect.

4.2. The relationship between contamination level and resistivity of coatings for niobium coatings

Two specimens (Nb-A1 and Nb-A2) were deposited to test the correlation of resistivity and coating impurity levels. As stated in the procedure, impurity level was regulated using a controlled leak and an Inficon residual gas analyzer. The results of the scans are given below. Overall, the resistivity scans indicate a fairly uniform value across the samples. There is a much more visible correlation between resistivity and background gas pressure than there is for the case of sputtering pressure. As expected, there is an increase in resistivity of the coatings as background gas pressure is increased. For a residual impurity level of 5% process gas, there is greater than a factor of two increase in resistivity. For 10% process gas impurity levels, there is approximately a factor of six increase. This indicates that the eddy current decay method of resistivity measurement is extremely sensitive to coating contamination levels (Fig. 12).

To ensure that the change in resistivity is in fact due to changes in impurity content and is not strongly affected by changes in porosity, topographic images that were taken are shown in Fig. 13. As indicated in Fig. 13, the coating is a near fully dense structure similar to that of the other specimens sputtered at 10 mTorr. This indicates that the resistivity changes are indeed due solely to the change in impurity contents and not changes in density. The changes in resistivity associated with rising impurity level are most

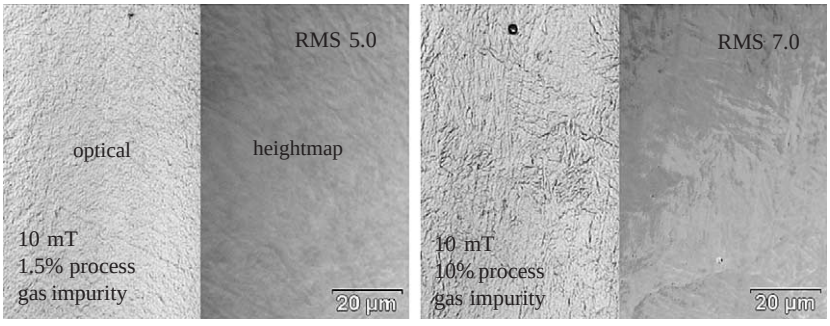

Fig. 13. Composite optical and topographic heightmap images as measured by laser scanning confocal microscopy. The sputtering pressure, surface finish and impurity level are given for each image. With very little change in surface finish.

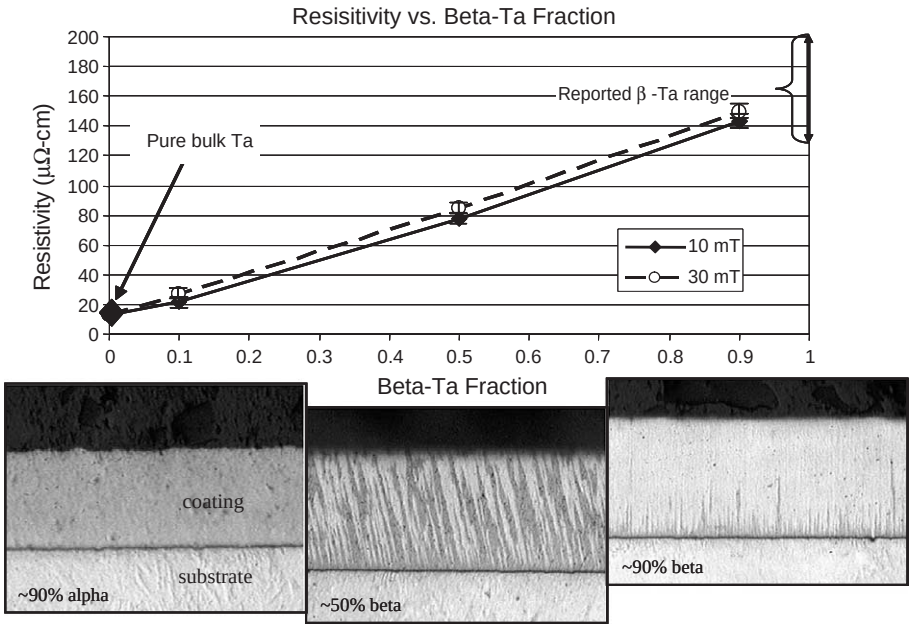

Fig. 14. Chart of resistivity vs. beta-Ta fraction for tantalum samples along with representative cross-sections of the coatings taken at areas of varying beta-Ta concentration. The lighter phase denotes alpha-Ta and the darker phase, beta-Ta. Resistivity varies linearly with beta-Ta concentration.

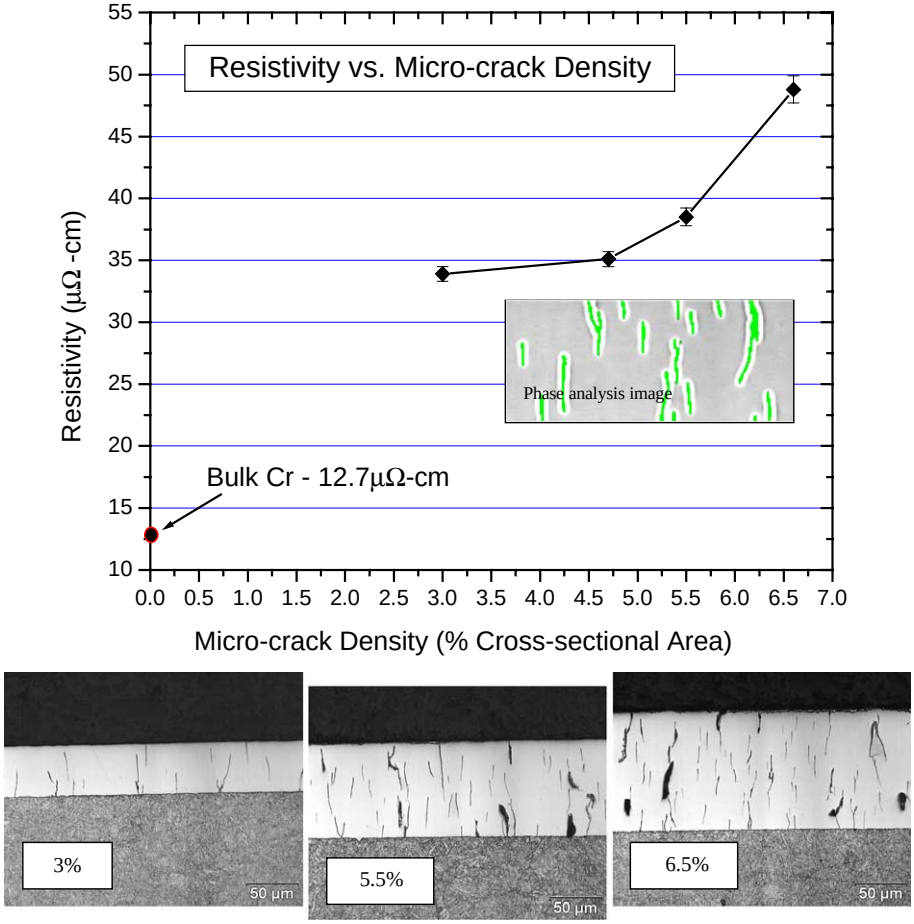

Fig. 15. Chart of resistivity vs. micro-crack density for chromium samples along with representative cross-sections of each coating. With increasing coating thickness, the micro-crack density increases along with the resistivity. Resistivity measurements corrected for thickness.

likely due to increases in lattice strain from interstitial nitrogen and oxygen as well as development of secondary nitride and oxide phases.

4.3. The relationship between tantalum coating phase and resistivity

Two specimens (Ta-1 and Ta-2) were deposited to test the correlation of resistivity and beta-Ta concentrations in magnetron sputtered tantalum.

The resistivity scan indicates that the resistivity measurement is very sensitive to beta-Ta concentration. This is to be expected considering there is an order of magnitude difference in resistivity of alpha-Ta and beta-Ta. To correlate the approximate beta-Ta fraction to the resistivity measurements, metallographic cross-sections were taken and analyzed (shown in Fig. 14). The darker phase in the image in Fig. 14 corresponds to the softer alpha-Ta while the lighter phase corresponds to beta-Ta. The approximate beta-Ta fractions are extrapolated from the cross-sections by an image analysis system and cross-referenced to their positions on the resistivity scans. The results are given in the chart below. Overall, the resistivity of the sample sputtered at 30 mTorr was slightly higher than that sputtered at 10 mTorr for a given beta-Ta fraction. This is similar to the results achieved with the niobium samples and is likely due to slight changes in coating density.

4.4. The relationship between cracking, porosity and resistivity of thick electroplated chromium coatings

Four specimens of electroplated chromium were completed to determine the correlation between micro-crack density and resistivity. Overall the changes in resistivity were subtle. This is similar to the changes in resistivity observed with changes in coating density, which is not surprising since the phenomenon for resistivity change is nearly identical. That is, the changes in resistivity are essentially due to changes in effective porosity of the coating. The cracks themselves act similarly to open grain boundaries and this empty volume will act to increase the "measured" resistivity but not the actual resistivity of the intact coating.

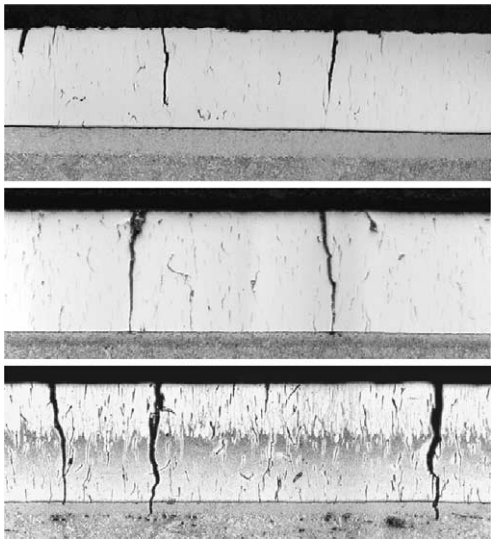

Fig. 16. Electroplated HC–Cr Damage Progression in a gun tube erosion simulator. Cross-sectional images taken at 4 shots, 12 shots and 34 shots respectively. The number of large cracks accompanied by subsequent widening will result in changes in resistivity.

Table 2
Average thickness and resistivity, the errors represent one standard deviation

Material	Sample	Average thickness (μm)		Average resistivity (μΩ cm)	
Nb	Nb-A1	40.8±0.7		86.9±3.1	
Nb	Nb-A2	15.9±0.5		37.0±1.5	
Nb	Nb-1	47±1.5		14.7±0.5	
Nb	Nb-2	58±4		17.5±0.7	
Nb	Nb-3	35±4		32.3±5.8	
HC–Cr	Cr-1	44±1		33.9±0.6	
HC–Cr	Cr-2	72±2		35.1±0.6	
HC–Cr	Cr-3	89±3		38.5±0.7	
HC–Cr	Cr-4	137±7		48.8±1.1	
		Alpha phase	Beta phase	Alpha phase	Beta phase
Ta	Ta-1	14±2	29±5	22.7±1.1	149±12
Ta	Ta-2	14±2	30±3	22.2±1.1	143±11

Fig. 15 illustrates the overall relationship between micro-crack density as measured by percentage cross-sectional area and resistivity. In addition, micrographs are given of several chromium coatings of varying thickness and micro-crack density.

The importance of this relationship can be directly related to the progression of damage in electroplated chromium gun tubes. Fig. 16 illustrates the crack widening effect that occurs upon repeated thermal cycles as experienced in gun tubes. This crack widening results in more rapid erosion of the steel interface due to increased vulnerability to the hot propellant gases. This effect should also be accompanied by a change in resistivity that can be measured via eddy current. In this mode, the eddy current method may be utilized to monitor coating degradation levels in the field to determine subsequent wear and erosion life.

4.5. Summary of resistivity measurement results

Table 2 gives a summary of resistivity measurements acquired for all the niobium, tantalum and chromium samples. The measurements obtained from our 2D scanner and reported here are the average and standard deviations of each sample.

5. Summary and conclusion

A dual-probe resistivity scanner based on eddy currents was designed and constructed. It was used to determine the

resistivity of niobium, tantalum and chromium coatings. The results obtained from the limited sample sets (Ta, Nb and Cr coatings) are in good agreement with other published measurements with other approaches. The pulsed eddy current method was used to develop a technique that allows very fast data acquisition rates with up to 10^5 samples per second. Even a data acquisition rate of 200 samples per second provides enough information for sample scanning and this rate was utilized in our experiments. This fast scanning capability makes this method useful for coating diagnostics during the manufacturing process as well as in the field.

In support of the robust and reliable method developed, the following correlations were made: the relationship of impurity level to resistivity is quite dramatic and is easily differentiated utilizing eddy current. The resistivity of niobium coatings vs. sputtering pressure does not follow a linear path. However, based on LSCM results, the resistivity maps of niobium coatings correlate well with density. Excellent correlation was obtained with resistivity data taken from samples of varying beta-Ta concentration. Resistivity values of tantalum coatings are in good agreement with literature [7,10]. Strong correlation between HC–Cr crack density and resistivity was found. This is useful for both QC testing and measuring coating degradation levels in the field.

References

[1] John C. Moulder, Erol Uzal, James H. Rose, Rev. Sci. Instrum. 63 (6) (1992 June).
[2] Cheng-Chi Tai, James H. Rose, John C. Moulder, Rev. Sci. Instrum. 67 (11) (1996 June).
[3] B. Lebrun, Y. Jayet, J. Baboux, NDT E Int. 30 (3) (1997) 163.
[4] T. Clauzon, F. Thollon, A. Nicolas, IEEE Trans. Magn. 35 (3) (1999 May).
[5] S. Giguere, B. Lepine, J.M.S. Dubbis, Res. Nondestr. 13 (2001) 119.
[6] Y. Danon, C. Lee, ASNT Spring Conference, 2003 (March), p. 40.
[7] Yaron Danon, Changqing Lee, Chris Mulligan, Greg Vigilante, IEEE Trans. Magn. 40 (4) (2004 July) 1826.
[8] Jack Blitz, Electrical and Magnetic Methods of Non-destructive Testing, Second edition, Chapman & Hall, 1997.
[9] J.A. Thornton, J. Vac. Sci. Technol., A 4 (6) (1986) 3059.
[10] L.A. Clevenger, A. Mutscheller, J.M.E. Harper, C. Cabral Jr., K. Barmak, J. Appl. Phys. 72 (10) (1992) 4918.
[11] S.L Lee, D. Windover, M. Audino, D.W. Matson, E.D. McClanahan, Surf. Coat. Technol. 149 (2002) 62.
[12] Philippe Catania, Ronnen A. Roy, Jerome J. Cuomo, J. Appl. Phys. 74 (2) (1993) 1008.
[13] C.C. Cheng, C.V. Dodd, W.E. Deeds, Int. J. Nondestr. Test. 3 (1971) 109.
[14] J.A. Thornton, Annu. Rev. Mater. Sci. 7 (1977) 239.
[15] K.H. Muller, J. Appl. Phys. 62 (1987) 1796.